Asian Journal of Chemistry; Vol. 37, No. 3 (2025), 707-714

ASIAN JOURNAL OF CHEMISTRY

https://doi.org/10.14233/ajchem.2025.33255

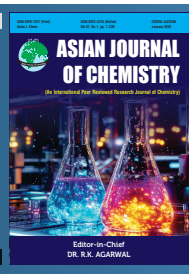

Effective, Reusable Applications of Nanostructured Silver-MnO_2 for Dye Degradation under UV Light and Dye-Sensitized Solar Cells

S. CHINNADHURAI[1], M. AROCKIA DOSS[2] and J. KAMALAKKANNAN[1,*]

[1]PG & Research Department of Chemistry, Sri Vinayaga College of Arts and Science (Affiliated College of Thiruvalluvar University), Ulundurpet-606107, India
[2]Department of Chemistry, St. Joseph University, Nagaland-797115, India

*Corresponding author: E-mail: dr.jkamalakkannan@gmail.com

Received: 23 December 2024; *Accepted*: 12 February 2025; *Published online*: 28 February 2025; AJC-21928

Silver-MnO_2, a metal-doped semiconductor oxide, was synthesized using a simple precipitation technique and characterized with XRD, FESEM, HR-SEM, TEM, EDS, UV-Vis DRS and PL spectroscopy. The XRD and EDS results confirmed that MnO_2 and metallic silver (Ag) are present in the catalyst, whereas FESEM images revealed a blend of nanoparticles with many cavities and hexagonal nanosheets. The HR-SEM and TEM analyses indicated that MnO_2 particles have a pentagonal or hexagonal shape with silver clusters on their smooth surfaces. Interestingly, Ag-MnO_2 absorbed more light in both the UV and visible areas compared to pure MnO_2. The photocatalytic performance of Ag-MnO_2 was evaluated by breaking down Evans blue (EB) dye under UV light, it clearly outperformed single-component MnO_2 and two-component systems. The enhanced performance is attributed due to the effects of silver doping, which appear to facilitate improved charge separation and transfer within the catalyst. Additionally, Ag-MnO_2 demonstrated a high degree of stability and can be reused easily. Over the course of four cycles, the catalytic capacity with a minimal reduction is sustained. Moreover, this material was more hydrophobic than MnO_2, which could help with self-cleaning uses.

Keywords: Precipitation method, Photocatalysis, Antibacterial activity, Evans blue dye, Dye-sensitized solar cell.

INTRODUCTION

In recent years, the challenge of eliminating colours from textile wastewater, particularly those containing non-biodegradable dyes, has accelerated. Heterogeneous photocatalysis has recently been investigated as a technique for eliminating toxic pollutants from industrial discharge, as it converts contaminants into CO_2, H_2O and mineral acids [1-4]. A practical approach for treating and recycling aqueous wastewater involves the photocatalytic breakdown of various dyes in water using semiconductor oxides exposed to UV light [5,6]. Currently, organic dyes represent the primary category of pollutants found in wastewater from multiple industries. Literature has shown that wide-bandgap metal oxides like TiO_2 and ZnO can effectively degrade numerous organic pollutants when subjected to UV light [7-9]. Several groups have synthesized nano-/mesoporous materials and their uses have been explored [10-13].

The uptake of ultraviolet (UV) light by wide-band-gap semiconductors facilitates the formation of electrons and holes through electronic excitation occurring between theence and conduction bands. These charge carriers generated by light can move to the surface of the semiconductor and engage in redox reactions with molecules that are adsorbed [14,15]. For practical purposes, it is essential to create new catalysts that function effectively under UV light. Among them, MnO_2 stands out as a highly promising material, suitable for a variety of advanced applications such as field-effect transistors, lasers, photodiodes, chemical and biological sensors and solar cells [16,17]. This effectiveness surpasses that of larger bulk materials due to its increased surface area, smaller dimensions, fewer free electrons and potential quantum confinement effects. The superior photocatalytic performance of nanomaterials has been linked to their larger surface areas, the presence of more oxygen vacancies and their ability to enhance the diffusion and mass transport of reactant molecules [18,19].

Studies have indicated that MnO_2 demonstrates greater efficacy than MnO_2 in treating effluents from the paper industry

and in decolourizing dyes [20-22]. Several strategies to modify MnO_2 have been explored, including doping with metals or non-metals and surface alterations [23-25]. In this study, a straightforward precipitation method was employed to synthesize Ag-MnO_2 nanostructure. The performance of catalyst was evaluated using Evans blue (EB) dye. The resulting material exhibited remarkable performance, robustness and high photocatalytic activity in breaking down EB dye when exposed to UV light.

EXPERIMENTAL

Silver nitrate ($AgNO_3$), manganese(II) nitrate tetrahydrate ($Mn(NO_3)_2{\cdot}4H_2O$), ammonia solution, nitric acid (65%), Evans blue (EB) dye and ruthenium dye (535-bisTBA, N719) were as received.

Synthesis of Ag-MnO_2 nanocomposite: The Ag-MnO_2 nanocomposite was prepared using a co-precipitation technique. Initially, 0.3 g of silver nitrate (0.1 M) dissolved in 20 mL of anhydrous ethanol was added slowly to 20 mL of $Mn(NO_3)_3{\cdot}4H_2O$ (2.68 g) solution while stirring vigorously at room temperature, ensuring that no precipitation occurred. Subsequently, aqueous ammonia and conc. HNO_3 were introduced dropwise to the mixture during vigorous stirring to bring the pH to approximately 9, which resulted in the formation of a precipitate. This precipitate was then filtered and washed with water and ethanol to remove any alkaline materials. Afterward, the solid was collected and dried in an oven at 100 ºC for 12 h in air. Finally, the powder obtained was calcined in a muffle furnace at 500 ºC for 3 h to produce the Ag-MnO_2 nanocomposite.

Characterization: UV-visible absorbance spectra in the range of 800-200 nm were obtained utilizing a Shimadzu UV-1650 spectrometer equipped with a 10 mm quartz cuvette. High-resolution scanning electron microscopy (HR-SEM) and energy dispersive X-ray (EDX) analysis were performed using a FEI Quanta FEG 200 apparatus at room temperature (25 ºC). The size and structure the nanoparticles were confirmed through transmission electron microscopy (HR-TEM) using a PHILIPS CM200 instrument. X-ray diffraction (XRD) patterns were captured with a Pan Analytical X'PERT PRO diffractometer set at 40 kV and 30 mA, employing Cu$K\alpha$ radiation. Photoluminescence (PL) spectra at ambient temperature were acquired with a Perkin-Elmer LS 55 fluorescence spectrometer. The antibacterial efficacy was assessed *via* the disc diffusion technique by dissolving the test substance in DMSO at a concentration of 200 mg/mL for 30 min, with ciprofloxacin (10 mg/disc) acting as the positive control.

Photocatalysis studies: The photocatalytic performance of the Ag-MnO_2 nanocomposite was assessed through the photodegradation process of a dye. The UV lamp, emitting at 365 nm, served as light source for the reaction conducted at room temperature (303 K). In this experiment, 40 mL of aqueous suspension containing Evans blue (EB) dye at a concentration of 1×10^{-4} M was combined with 0.060 g of photocatalyst in a 50 mL reaction tube. Before irradiation, the mixture was stirred magnetically in the dark for 60 min to establish either an adsorption or desorption equilibrium. The mixture was maintained under a continuous air-equilibrated environment. At specified intervals during the irradiation, the absorbance of suspension was measured spectrophotometrically, under the Beer-Lambert law.

RESULTS AND DISCUSSION

SEM-EDX analysis: To examine the distribution of Mn and O on the surface of pure MnO_2, the elemental mapping utilizing SEM was conducted. As observed in Fig. 1a, the FE-SEM image reveals a mixture of criss-crossed sheet-like shapes

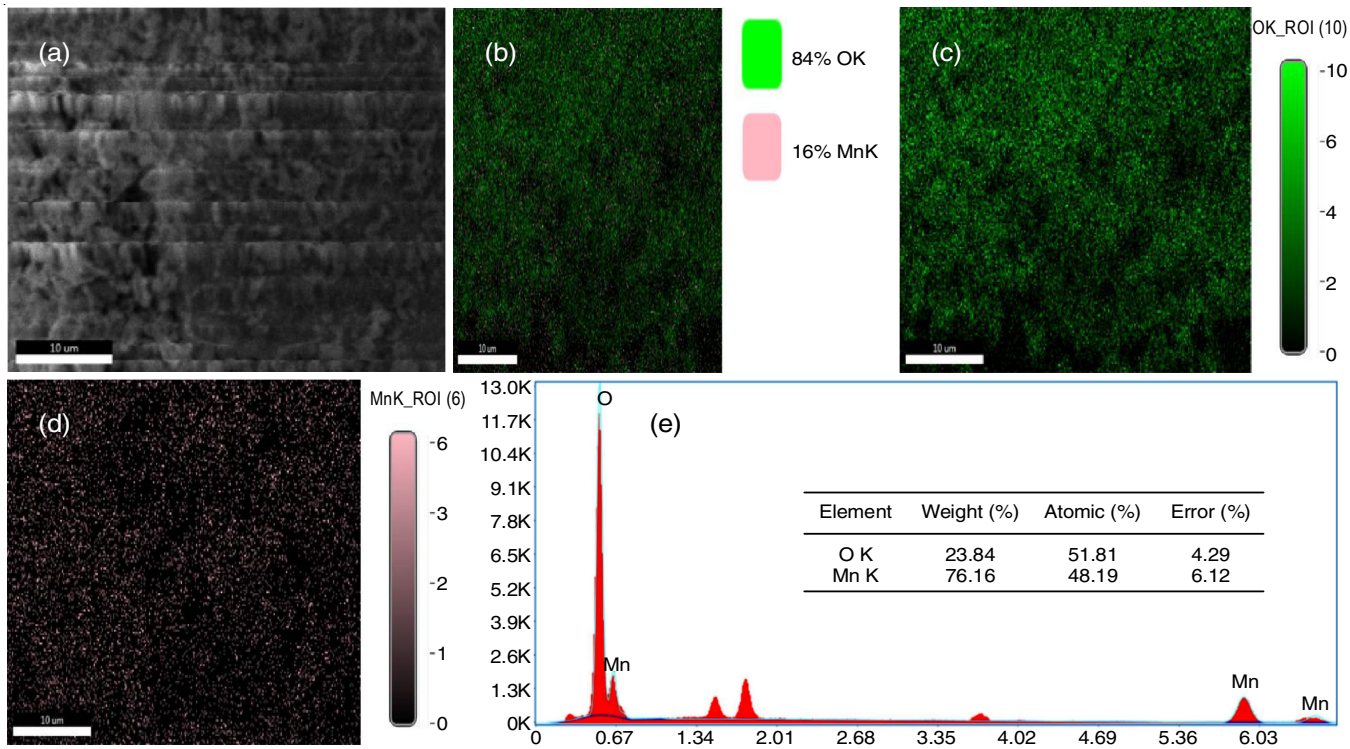

Fig. 1. FE-SEM: (a) image elemental mapping of MnO_2, (b) elemental mapping of FE-SEM, (c) Mn, (d) O and (e) EDX analysis

and nanobundles of MnO_2, whereas Fig. 1b-d shows the elemental mapping with different colours for Mn (pink) and O (green). The FE-SEM image of silver doped MnO_2 (Fig. 2a) semiconductor oxide shows the intercrossed flower-like patterns. In Fig. 2b-g, it becomes clear that Ag (red), Mn (pink) and O (green) spread out evenly across the catalyst. It is interesting to observe that the amounts of Mn and O exceed those of Ag. The EDX spectra (Fig. 1e & 2h) also to confirm the presence of these elements in respective materials.

HR-TEM analysis: The HR-TEM image of Ag-MnO_2 semiconductor oxide at 10 nm shows a clear hexagonal structure (Fig. 3a). A 2D surface plot (Fig. 3b) presents a 3D structure of the prepared Ag-MnO_2 material. The Image J Viewer' program [26] points out the selected particle, which also displays the length of this chosen particle's area (Fig. 3c).

Optical studies: The optoelectronic characteristics of the prepared heterostructured Ag doped MnO_2 were investigated through diffuse reflectance UV-Vis spectroscopy and photoluminescence (PL). The diffuse reflectance spectra showed that Ag-MnO_2 has a way higher absorption in the ultraviolet range (200–400 nm) than MnO_2 (Fig. 4), which indicates that enhanced performance in photocatalytic activity when exposed to UV light. In the visible region, there was an increase in absorption, likely due to the interaction with Ag, which probably aligns the energy levels nearer to the conduction band or valence band edges of MnO_2, enhancing absorption in both UV and visible regions. The bandgap energies were found to be 3.3 eV for MnO_2 and 3.1 eV for Ag-MnO_2 (Fig. 5a-b), indicating that Ag-MnO_2 has a slightly lower bandgap energy, thereby improving its absorption peak and establishing it as a highly promising and cost-effective photocatalyst.

Photoluminescence: Fig. 6a-b illustrate the photoluminescence spectra of MnO_2 and the synthesized Ag-MnO_2 heterojunction. The material emits a near UV emission band, which

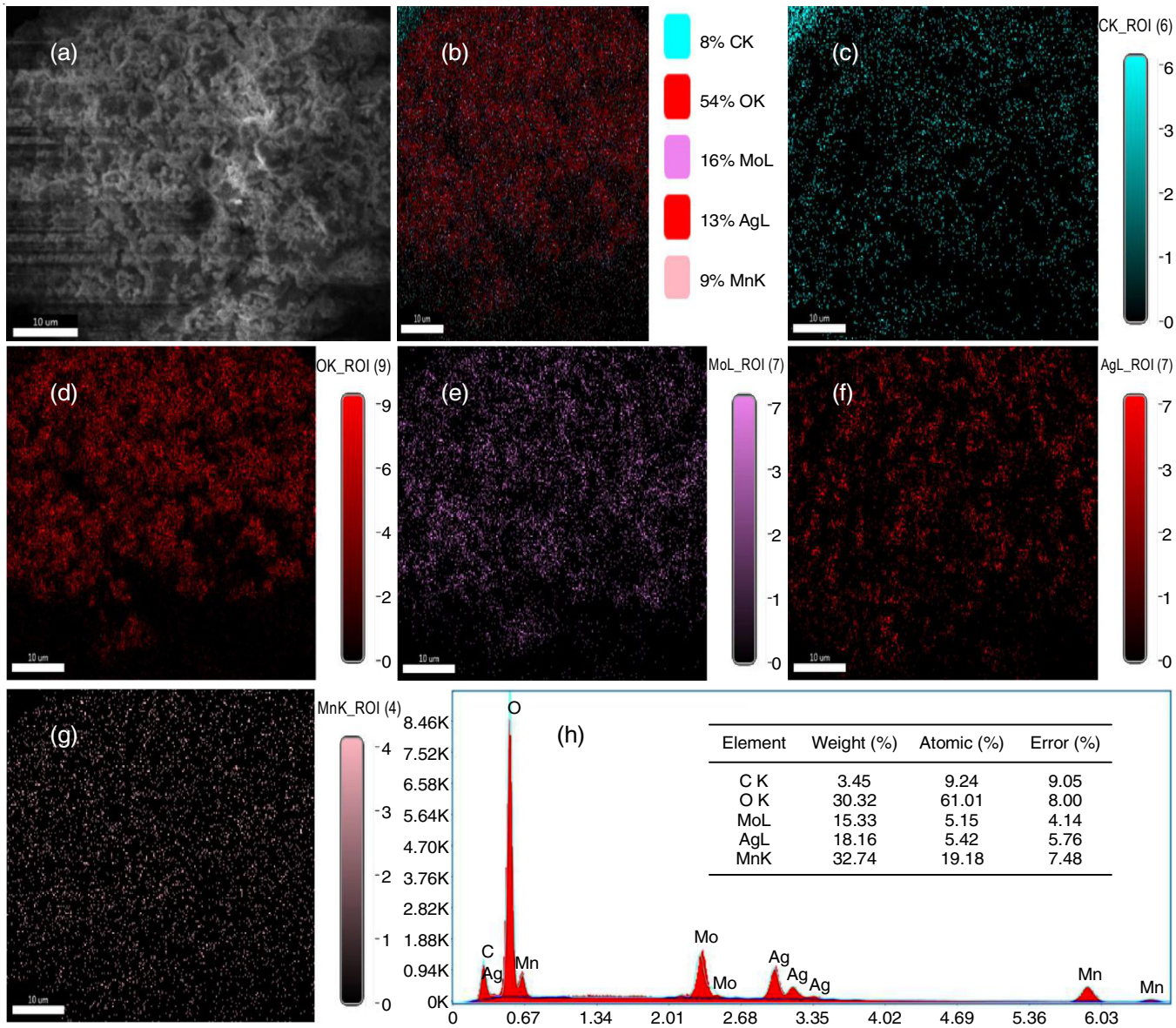

Element	Weight (%)	Atomic (%)	Error (%)
C K	3.45	9.24	9.05
O K	30.32	61.01	8.00
MoL	15.33	5.15	4.14
AgL	18.16	5.42	5.76
MnK	32.74	19.18	7.48

Fig. 2. FE-SEM: (a) image. elemental mapping of Ag-MnO_2, (b) elemental mapping of FE-SEM, (c) C, (d) O, (e) Mo, (f) Ag, (g) Mn and (h) EDX analysis

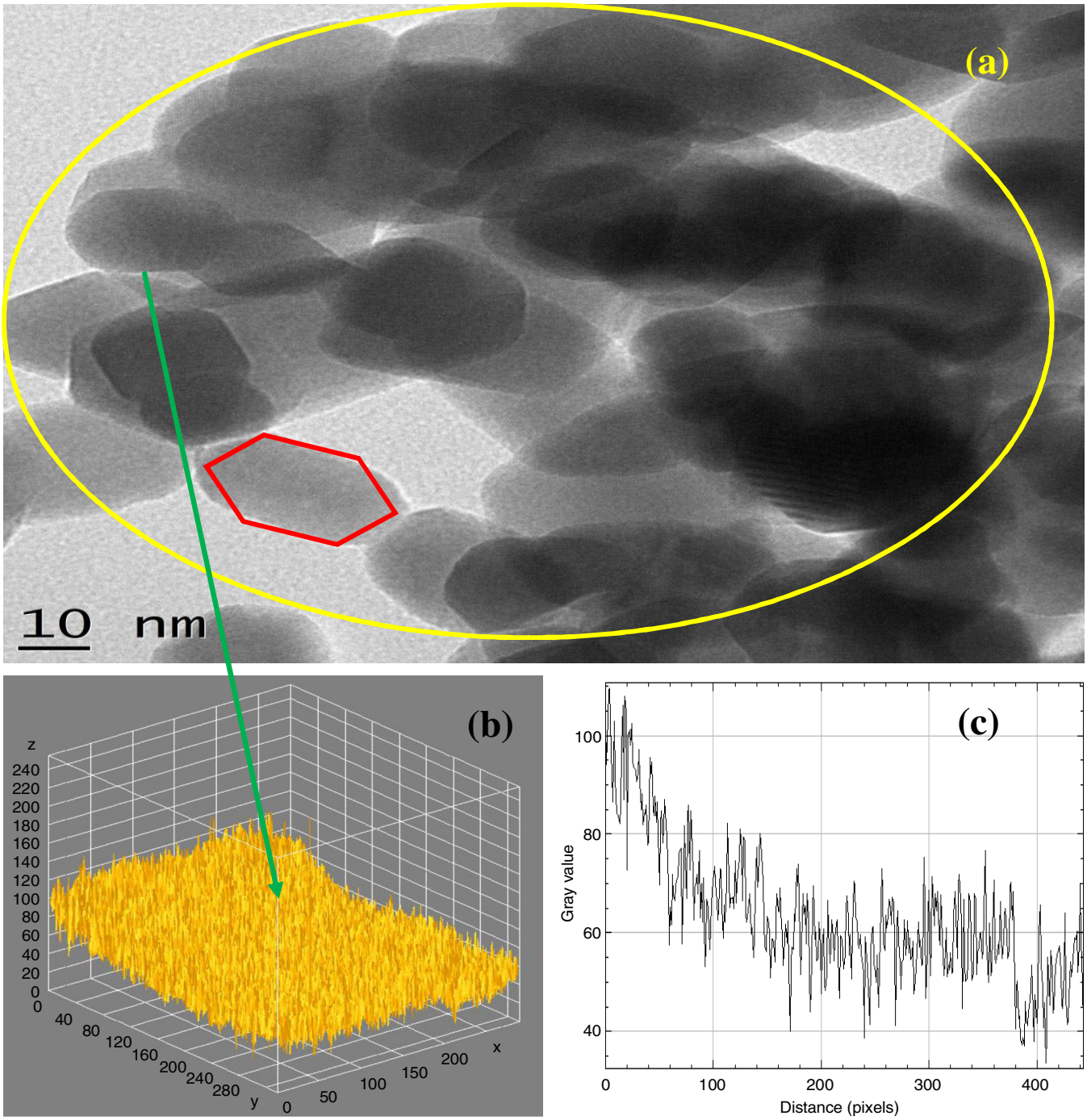

Fig. 3. HR-TEM: Ag-MnO_2 (a) image (b) interactive 3D structure and (c) plot profile by selected particle region painted fig (a)

is quite interesting and observed that the photoluminescence intensity of Ag-MnO_2 is not as prominent as that of MnO_2. This near UV light is linked with exciton recombination related to near-band edge emission of MnO_2 [27-30]. The comparison of Ag-MnO_2 with MnO_2 alone demonstrates that the presence of Ag on MnO_2 suppresses the recombination of photogenerated electron-hole pairs and this inhibition can improve photocatalytic activity, which is advantageous in such materials.

Photodegradation of dye: Fig. 7 illustrates the photocatalytic breakdown of Evans blue dye under optimized conditions. Since dye is resistant to self-photolysis, a slight (4%) reduction in dye cosncentration was observed under same conditions conducted in dark employing Ag-MnO_2. Under natural sunlight, Evans blue dye degrades by 95% within 60 min in the presence of Ag-MnO_2. Whereas developed MnO_2 and without catalyst yielded 59% and 6% degradation, respectively.

Effect of pH: The effect of initial pH (Fig. 8) illustrates the percentages of dye degradation for Evans blue dye across a pH range of 3 to 12. The degradation rate increases until the pH reaches 11, after which it declines. Thus, pH 11 is optimized as the optimal pH for Evans blue dye. The acid-base properties of the metal oxide surface can profoundly influence the photo-

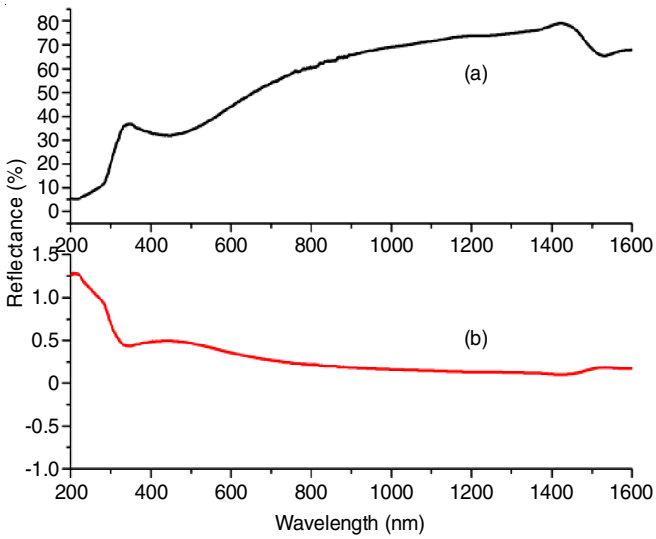

Fig. 4. DRS of (a) prepared MnO_2 and (b) Ag-MnO_2 nanocomposite material

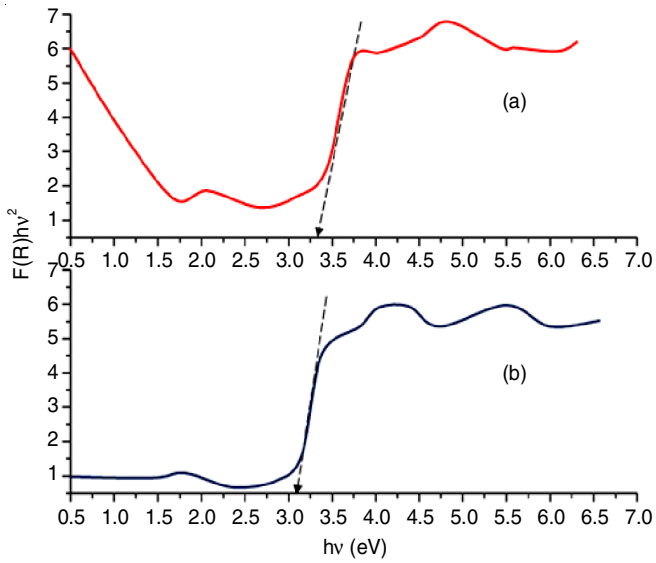

Fig. 5. UV-Vis DRS-direct band gap of (a) prepared MnO_2 and (b) Ag-MnO_2 nanocomposite material

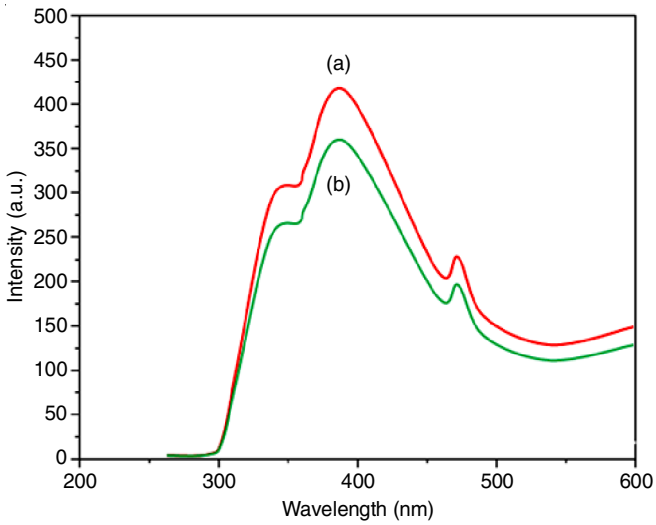

Fig. 6. PL spectrum of (a) prepared MnO_2 and (b) Ag-MnO_2 nanocomposite material

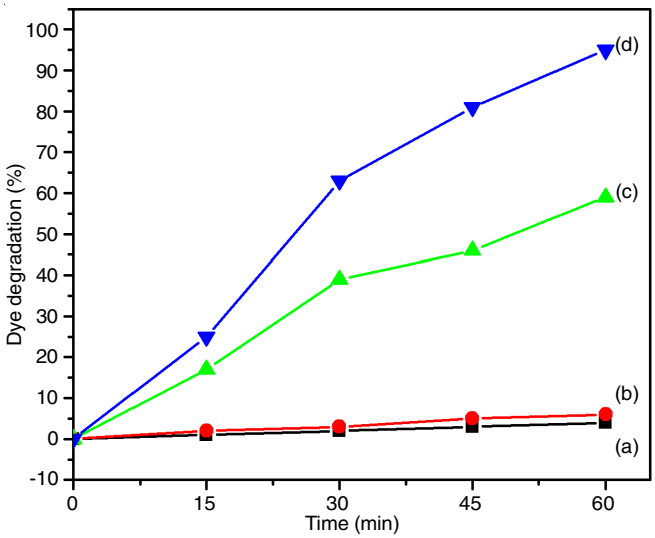

Fig. 7. Effect of degradation study of EB dye under UV-light irradiation by (a) without catalysis (b) dark (c) MnO_2 and (d) Ag-MnO_2 nanocomposite material

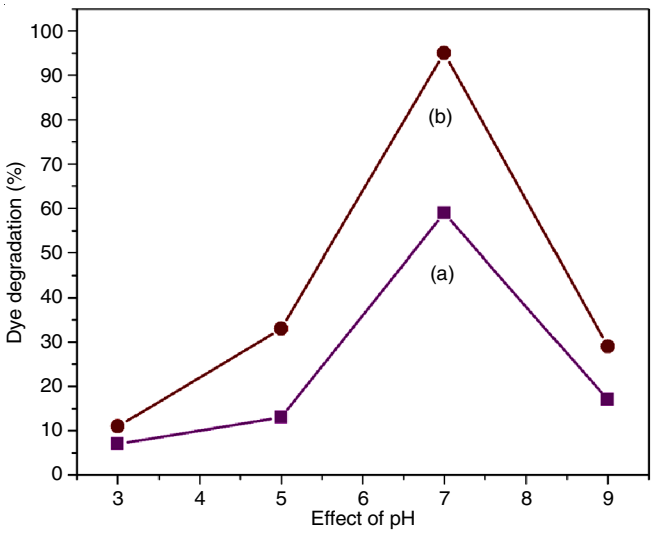

Fig. 8. Effects of pH (a) prepared MnO_2 and (b) Ag-MnO_2 nanocomposite material

catalytic ability of the material. The oxidizing agent responsible for dye degradation, hydroxyl radical, is more readily produced at high pHs [31,32].

Effect of catalyst loading: The experimental results indicated that the photodegradation efficiency of Ag-MnO_2 material increased to 0.06 g per 50 mL, after which it exhibited a decline with further catalyst loading. The synthesized MnO_2 and Ag-MnO_2 demonstrated photodegradation percentages of 59% and 95% for the Evans blue dye, respectively (Fig. 9). As the catalyst dosage increases, the active surface area rises however, an excess dosage leads to a decrease in solar light diffusion due to particle interactions [33,34]. This results in a reduced photocatalytic activated volume of suspension. Moreover, it is essential to maintain low treatment levels for industrial application purposes.

Effect of concentrations: At varying concentrations of Evans blue dye, Fig. 10 illustrates that at the concentration of 1×10^{-4} M leads to the maximum photodegradation as compared

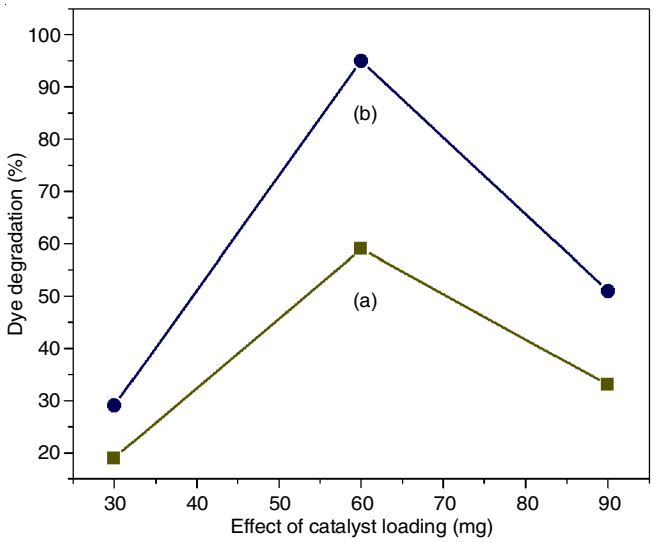

Fig. 9. The effects of catalyst loading EB dye under UV-light irradiation at 365 nm by (a) prepared MnO_2 and (b) Ag-MnO_2 nanocomposite material

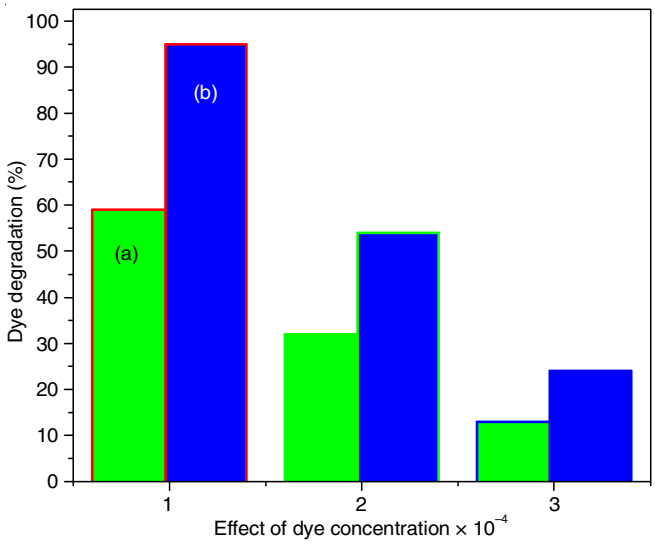

Fig. 10. Effects of concentrations of (a) prepared MnO_2 and (b) Ag-MnO_2 nanocomposite material

to other studied high concentrations. The results demonstrate that a high concentration of Evans blue dye molecules reduces the degradation range. The decrease in activity results from its effect on the catalyst, particularly MnO_2 and Ag-MnO_2, which reduces their surface area, while elevated quantities hinder photocatalytic activity relative to lower concentrations of dye molecules.

Selection of oxidants: The generation of molecular oxygen is commonly utilized as an electron acceptor in the heterogeneous photocatalytic processes. In general, the irreversible electron acceptors such as KIO_4, $H_3K_5O_{18}S_4$ (oxone) and $KBrO_3$ are used to generate molecular oxygen in order to mitigate the electron-hole recombination [35,36]. Thus, in this work, the effects of three different oxidizing agents *viz*. $KBrO_3$, $H_3K_5O_{18}S_4$ (oxone) and $KBrO_3$ were investigated on the degradation of Evans blue dye. It appears that the addition of these oxidants enhances the photodegradation of Evans blue dye, as shown in Fig. 11. Peroxymonosulfate ($HOOSO_3^-$), often referred to as oxone and popularly known as HSO_5^-, has been utilized as an oxidant in light-driven processes under specific conditions. The primary reason for enhanced degradation with these oxidants is their ability to generate highly reactive radical intermediates and to capture electrons (eqns. 1-5). This activity may further enhance the photocatalytic degradation of the dye [37,38].

$$IO_4^- + h\nu \longrightarrow IO_3^{\bullet} + O^{\bullet-} \quad (1)$$

$$O^{\bullet-} + H^+ \longrightarrow {}^{\bullet}OH \quad (2)$$

$$HSO_5^- \longrightarrow SO_4^{\bullet-} + {}^{\bullet}OH \quad (3)$$

$$SO_4^{\bullet-} + H_2O \longrightarrow {}^{\bullet}OH + SO_4^{2-} + H^+ \quad (4)$$

$$BrO_3^- + 6e_{CB}^- + 6H^+ \longrightarrow Br^- + 3H_2O \quad (5)$$

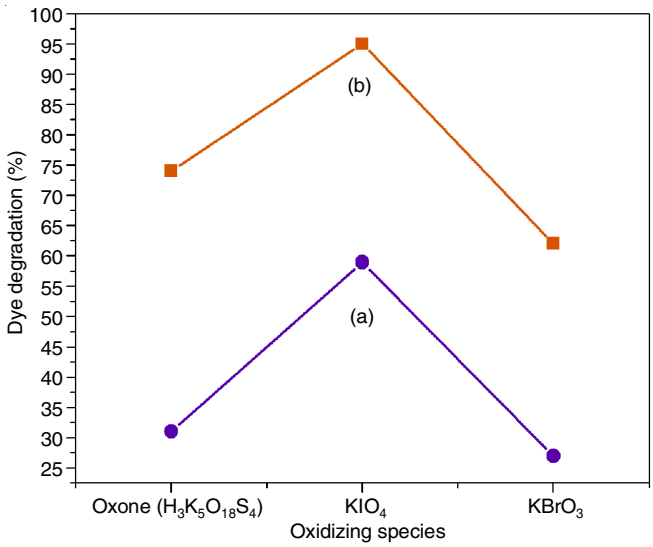

Fig. 11. Effects of oxidizing proceses of (a) prepared MnO_2 and (b) Ag-MnO_2 nanocomposite material {[SY] = 3×10^{-4} mol/L; pH = 7 ± 0.1; 13.4 wt.% catalyst suspended = 4 g L^{-1}; Oxidants = 0.01 M; irradiation time = 60 min; airflow rate = 8.1 mL s^{-1}; $I_{UV} = 1.381 \times 10^{-6}$ Einstein L^{-1} s^{-1}}

It is subsequently found that KIO_4 is more potent than other oxidants in accelerating the degradation of Evans blue dye and the activity is observed to be in the following order:

$$KIO_4 > H_3K_5O_{18}S_4 > KBrO_3$$

Chemical oxygen demand (COD) analysis: The COD measurements were performed for the degradation of Evans blue dye using Ag-MnO_2 catalyst under ideal conditions. After 30 and 60 min of irradiation, respectively, the COD value of 4240 ppm for 1×10^{-4} mol/L of Evans blue dye concentration steadily decreases to 960 ppm and 240 ppm (Fig. 12). After 60 min, there was 95.30% COD reduction for EB dye under UV light. The generation of CO_2 during photodegradation also provided evidence of colour mineralization. By passing the evolved gas produced during photodegradation into limewater, the generation of carbon dioxide was tested.

Reusability of catalyst: By employing the used catalyst to carry out the degradation, the reusability of the catalyst was investigated. For four cycles, the MnO_2 and Ag-MnO_2 showed excellent photostability with no discernible loss of photo-

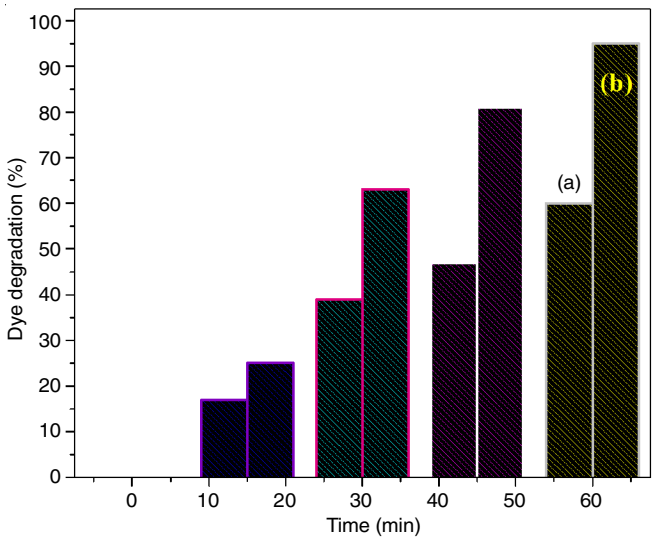

Fig. 12. Effects COD analysis

catalytic activity (Table-1). Even though MnO_2 and Ag-MnO_2 degradation efficiency decreases with each run, the catalyst demonstrated 93, 89, 89% and 97, 92, 92% activity during the second, third and fourth cycles, respectively. These findings confirmed that Ag-MnO_2 catalyst is highly useful and reusable when exposed to UV radiation.

TABLE-1
CATALYST REUSABILITY

Number of cycles	EB removal MnO_2 (%)	EB removal Ag-MnO_2 (%)
1	100	100
2	93	97
3	89	92
4	89	92

Mechanism: Scheme-I illustrates the mechanistic process of Ag-MnO_2 photocatalyst, which facilitates charge separation and functions in photocatalytic activity. When a semiconductor encounters solar radiation, a valence-band electron (VB) transitions to the conduction band (CB), resulting in the formation of a hole in the valence band. Usually, semiconductors diminish their photocatalytic activity due to electron-hole recombination [39]. In this nanostructure material, silver captures electrons from the conduction band of MnO_2, thereby inhibiting the recombination. Through electron trapping, silver can contribute to the inhibition of electron and positive hole recombination. As the silver ability to capture radicals increases the formation of superoxide radical anions. Furthermore, water and the vacant bonding sites of MnO_2 interact to produce extremely reactive hydroxyl ($^{\bullet}OH$) radicals. Thus, the dye molecules degraded by hydroxyl radicals and superoxide radical anions. The increase in $O_2^{\bullet-}$ generation, attributed to Ag, could enhance the photocatalytic activity of Ag-MnO_2.

Photovoltaic properties: The photocurrent voltage (I-V) behaviour for the dye-sensitized solar cells (DSSCs) fabrication is shown in Fig. 13. As a photoelectrode, the MnO_2 and AgO_2 nanocomposite materials were placed on a glass substrate that has been doped with fluorine, also known as an FTO-plate.

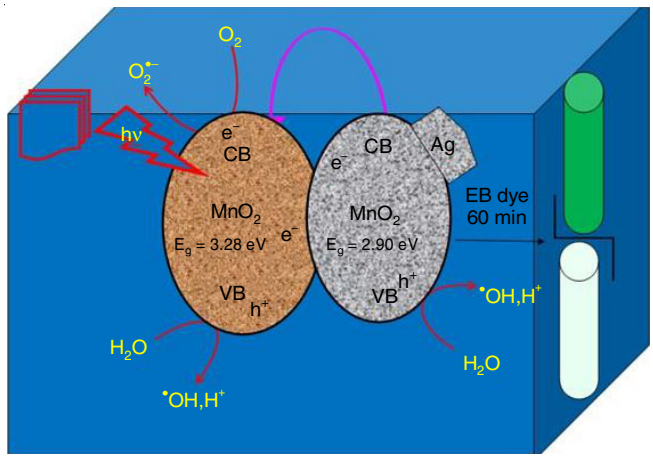

Scheme-I: Schematic representation for the photodegradation holes and electrons in the Ag-MnO_2 nanocomposite material under UV-light for successive mineralization of EB dye

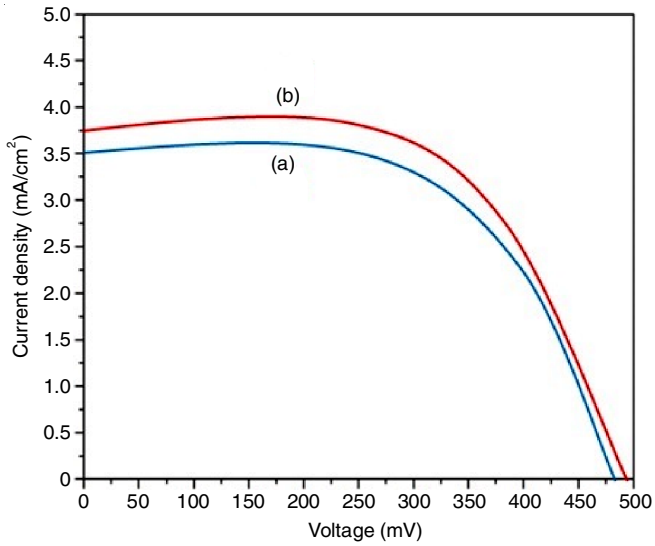

Fig. 13. Current density-voltage (I-V) curves for the DSSC's fabricated from prepared MnO_2 and (b) Ag-MnO_2 nanocomposite material

The standard solar cell was made using MnO_2 and Ag-MnO_2 nanocomposite in conjunction with ruthenium dye (535-bisTBA, N719). Based on the results, it appears that the Ag-MnO_2 nanocomposite material-based cell (N719) accomplishes the largest short-circuit current density when dyes are used as a sensitizer. Compared to MnO_2, which has a lower J_{sc} value of 3.5 mA/cm^2, Ag-MnO_2 has a higher value of 3.8 mA/cm^2. The values of V_{oc} is 500 mV voltage, fill-factor (FF) is 0.94 and efficiency (η) is 1.7%, which demonstrates that the Ag-MnO_2 nanostructure materials are highly effective in transferring electrons and preventing the recombination of photogenerated charge carriers, which in turn raises short-circuit current and improves electron transfer [40,41].

Conclusion

A nanostructure material Ag-MnO_2 was prepared and found to have uniformly inter-crossed sheet-like structures, which was confirmed by FE-SEM imaging, whereas the HR-TEM image showed a hexagonal structure. Diffuse reflectance spectroscopy (DRS) analysis showed that Ag-MnO_2 has a lower band gap

energy than MnO_2, which makes better UV-active photocatalyst. Photoluminescence (PL) analysis revealed that Ag-MnO_2 had lower luminescence emission intensity, which connects to higher photocatalytic activity. The nanostructure Ag-MnO_2 demonstrated superior photocatalytic performance compared to MnO_2 in the degradation of Evans blue (EB) dye when exposed to 365 nm UV light. The nanostructure material proved to be stable and reusable, highlighting its significant potential as an effective photocatalyst for both environmental and industrial applications.

CONFLICT OF INTEREST

The authors declare that there is no conflict of interests regarding the publication of this article.

REFERENCES

1. G. Ren, H. Han, Y. Wang, S. Liu, J. Zhao, X. Meng and Z. Li, *Nanomaterials*, **11**, 1804 (2021); https://doi.org/10.3390/nano11071804
2. D. Friedmann, *Water*, **14**, 3588 (2022); https://doi.org/10.3390/w14213588
3. A.O. Ibhadon and P. Fitzpatrick, *Catalysts*, **3**, 189 (2013); https://doi.org/10.3390/catal3010189
4. N. Gaur, D. Dutta, A. Singh, R. Dube and D.V. Kamboj, *Front. Environ. Sci.*, **10**, 872514 (2022); https://doi.org/10.3389/fenvs.2022.872514
5. J. Iyyappan, B. Gaddala, R. Gnanasekaran, M. Gopinath, D. Yuvaraj and V. Kumar, *Case Stud. Chem. Environ. Eng.*, **9**, 100599 (2024); https://doi.org/10.1016/j.cscee.2023.100599
6. S. Tak, S. Grewal, Shreya, P. Phogat, Manisha, R. Jha and S. Singh, *Chem. Eng. Technol.*, **47**, e202400142 (2024); https://doi.org/10.1002/ceat.202400142
7. S. Lam, J. Sin, A.Z. Abdullah and A.R. Mohamed, *Desalination Water Treat.*, **41**, 131 (2012); https://doi.org/10.1080/19443994.2012.664698
8. B. Krishnakumar and M. Swaminathan, *Spectrochim. Acta A Mol. Biomol. Spectrosc.*, **81**, 739 (2011); https://doi.org/10.1016/j.saa.2011.07.019
9. M. Muruganandham, N. Shobana and M. Swaminathan, *J. Mol. Catal. Chem.*, **246**, 154 (2006); https://doi.org/10.1016/j.molcata.2005.09.052
10. Y. Yamauchi, *J. Ceram. Soc. Jpn.*, **121**, 831 (2013); https://doi.org/10.2109/jcersj2.121.831
11. H. Oveisi, S. Rahighi, X. Jiang, Y. Nemoto, A. Beitollahi, S. Wakatsuki and Y. Yamauchi, *Chem. Asian J.*, **5**, 1978 (2010); https://doi.org/10.1002/asia.201000351
12. T. Kimura, Y. Yamauchi and N. Miyamoto, *Chem. Eur. J.*, **17**, 4005 (2011); https://doi.org/10.1002/chem.201002939
13. T. Kimura, Y. Yamauchi and N. Miyamoto, *Chem. Eur. J.*, **16**, 12069 (2010); https://doi.org/10.1002/chem.201001251
14. E. Monroy, F. Omnès and F. Calle, *Semicond. Sci. Technol.*, **18**, R33 (2003); https://doi.org/10.1088/0268-1242/18/4/201
15. F. Cao, Y. Liu, M. Liu, Z. Han, X. Xu, Q. Fan and B. Sun, *Research*, **7**, 0385 (2024); https://doi.org/10.34133/research.0385
16. D.V. Rupnar, S.A. Mane, H. Razi, V.H. Goswami, B.G. Pawar, P.B. Sarwade and N.S. Ramgir, *Inorg. Chem. Commun.*, **173**, 113784 (2025); https://doi.org/10.1016/j.inoche.2024.113784
17. M. Diantoro, I. Istiqomah, Y. Al-Fath, N. Nasikhudin, Y. Alias and W. Meevasana, *Int. J. Appl. Ceram. Technol.*, **20**, 2077 (2023); https://doi.org/10.1111/ijac.14377
18. A. McLaren, T. Valdes Solis, G. Li and S.C. Tsang, *J. Am. Chem. Soc.*, **131**, 12540 (2009); https://doi.org/10.1021/ja9052703
19. N. Kislov, J. Lahiri, H. Verma, D.Y. Goswami, E. Stefanakos and M. Batzill, *Langmuir*, **25**, 3310 (2009); https://doi.org/10.1021/la803845f
20. M.C. Yeber, J. Rodríguez, J. Freer, J. Baeza, N. Durán and H.D. Mansilla, *Chemosphere*, **39**, 1679 (1999); https://doi.org/10.1016/S0045-6535(99)00068-5
21. B. Krishnakumar and M. Swaminathan, *Indian J. Chem.*, **49A**, 1035 (2010).
22. B. Krishnakumar, K. Selvam, R. Velmurugan and M. Swaminathan, *Desalination Water Treat.*, **24**, 132 (2010); https://doi.org/10.5004/dwt.2010.1466
23. V. Etacheri, R. Roshan and V. Kumar, *ACS Appl. Mater. Interfaces*, **4**, 2717 (2012); https://doi.org/10.1021/am300359h
24. B. Subash, B. Krishnakumar, M. Swaminathan and M. Shanthi, *Mater. Sci. Semicond. Process.*, **16**, 1070 (2013); https://doi.org/10.1016/j.mssp.2013.04.001
25. J.F. Lu, Q.W. Zhang, J. Wang, F. Saito and M. Uchida, *Powder Technol.*, **162**, 33 (2006); https://doi.org/10.1016/j.powtec.2005.12.007
26. J. Kamalakkannan, V.L. Chandraboss, B. Loganathan, S. Prabha, B. Karthikeyan and S. Senthilvelan, *Appl. Nanosci.*, **6**, 691 (2015); https://doi.org/10.1007/s13204-015-0474-y
27. K. Vanheusden, W.L. Warren, C.H. Seager, D.R. Tallant, J.A. Voigt and B.E. Gnade, *J. Appl. Phys.*, **79**, 7983 (1996); https://doi.org/10.1063/1.362349
28. V. Srikant and D.R. Clarke, *J. Appl. Phys.*, **83**, 5447 (1998); https://doi.org/10.1063/1.367375
29. S.C. Lyu, Y. Zhang, H. Ruh, H. Lee, H. Shim, E. Suh and C.J. Lee, *Chem. Phys. Lett.*, **363**, 134 (2002); https://doi.org/10.1016/S0009-2614(02)01145-4
30. L. Bergman, X.B. Chen, J.L. Morrison, J. Huso and A.P. Purdy, *J. Appl. Phys.*, **96**, 675 (2004); https://doi.org/10.1063/1.1759076
31. S. Subramanian, J.S. Noh and J.A. Schwarz, *J. Catal.*, **114**, 433 (1988); https://doi.org/10.1016/0021-9517(88)90046-2
32. S. Balachandran, S.G. Praveen, R. Velmurugan and M. Swaminathan, *RSC Advances*, **4**, 4353 (2014); https://doi.org/10.1039/C3RA45381B
33. B. Krishnakumar, B. Subash and M. Swaminathan, *Sep. Purif. Technol.*, **85**, 35 (2012); https://doi.org/10.1016/j.seppur.2011.09.037
34. R. Velmurugan, K. Selvam, B. Krishnakumar and M. Swaminathan, *Separ. Purif. Tech.*, **80**, 119 (2011); https://doi.org/10.1016/j.seppur.2011.04.018
35. S.A. Naman, Z.A.A. Khammas and F.M. Hussein, *J. Photochem. Photobiol. Chem.*, **153**, 229 (2002); https://doi.org/10.1016/S1010-6030(02)00235-6
36. N. Daneshvar, D. Salari and A.R. Khataee, *J. Photochem. Photobiol. Chem.*, **162**, 317 (2004); https://doi.org/10.1016/S1010-6030(03)00378-2
37. S. Anandan, P. Sathish Kumar, N. Pugazhenthiran, J. Madhavan and P. Maruthamuthu, *Sol. Energy Mater. Sol. Cells*, **92**, 929 (2008); https://doi.org/10.1016/j.solmat.2008.02.020
38. B. Krishnakumar and M. Swaminathan, *Spectrochim. Acta A Mol. Biomol. Spectrosc.*, **81**, 739 (2011); https://doi.org/10.1016/j.saa.2011.07.019
39. M. Zhang, T. An, X. Hu, C. Wang, G. Sheng and J. Fu, *Appl. Catal. A Gen.*, **260**, 215 (2004); https://doi.org/10.1016/j.apcata.2003.10.025
40. Y. Zhang, L. Wang, B. Liu, J. Zhai, H. Fan, D. Wang, Y. Lin and T. Xie, *Electrochim. Acta*, **56**, 6517 (2011); https://doi.org/10.1016/j.electacta.2011.04.118
41. J. Kamalakkannan, V.L. Chandraboss, S. Prabha, B. Karthikeyan and S. Senthilvelan, *J. Mater. Sci. Mater. Electron.*, **015**, 4050 (2015); https://doi.org/10.1007/s10854-015-4050-8